PCCP

Accepted Manuscript

ROYAL SOCIETY OF CHEMISTRY

www.rsc.org/pccp

Journal Name

ARTICLE

Corrole-ferrocene & corrole-anthraquinone dyads: synthesis, spectroscopy and photochemistry

Received 00th January 20xx,
Accepted 00th January 20xx

DOI: 10.1039/x0xx00000x

www.rsc.org/

Jaipal Kandhadi,[a] Venkatesh Yeduru[ab] Prakriti R. Bangal[ab] and Lingamallu Giribabu*[ab]*

Two different Donor-Acceptor systems based on Corrole-Ferrocene and Corrole-Anthraquinone having '*Olefin Bridge*' at the β-pyrrole position have been designed and synthesized. Both the dyads Corrole-Ferrocene (**Cor-Fc**) and Corrole-Anthraquinone (**Cor-AQ**) are characterized by elemental analysis, ESI-MS, ^{1}H NMR, UV−visible, fluorescence spectroscopies (steady-state, femtosecond time-resolved), femtosecond transient absorption spectroscopy (*fs*-TA) and electrochemical methods. ^{1}H-NMR shows the two doublets at 6.50 and 7.25(δ) ppm is belongs to vinylic protons, which are characteristic for the formation of dyads. UV-Visible absorption spectra showed that dyads are merely superpositions of their respective constituent monomers and dominated by corrole $S_1 \leftarrow S_0$ (Q-band) and $S_2 \leftarrow S_0$(Soret band) transitions with systematic red-shift of both Soret and Q-bands along with brodening of the bands. A promiment spliting of the Soret band for both the dyads is observed due to bulky substitutions in the peripheral position which devaiate from the planarity of the corrole macrocycle. Both the dyads exhibit significant fluorescence emission quenching (95−97%) of the corrole emission compared to the free corrole monomer. The emission quenching is attributed to the excited-state intramolecular photoinduced electron transfer (PET) from corrole to anthraquinone in **Cor-AQ** dyad where as in **Cor-Fc** dyad it is reversed. The electron-transfer rates (k_{ET}) for Cor-AQ and **Cor-Fc** was found to be 3.33 x 10^{11} and 2.78 x 10^{10} s^{-1}, respectively. Despite their very diffrent driving forces, charge separation (CS) and charge recombination (CR) are found to be in identical timescales.

Introduction

Over the past years, considerable efforts has been devoted in the design, synthesis and scrutiny of donor-acceptor (D-A) systems for undergoing efficient intramolecular photoinduced electron transfer (PET) or excitation energy transfer (EET) and thus mimicking the reaction centre of natural photosynthetic organisms.[1−8] Among various systems, porphyrins are of particular importance as building blocks for the construction of models.[9-11] Porphyrins almost dominate the study of D-A systems, due to their easy availability and large body of information on their synthetic strategies and photophysical processes.[12-15] In spite of this many other porphyrinoids have interesting photophysical properties and have been used as photoactive components in the construction of models mimicking various stages of photosynthesis. For example phthalocyanines,[16,17] subphthalocyanines,[18] chlorins,[19] fused porphyrins,[20] core modified porphyrins,[21] expanded porphyrins,[22] contracted porphyrins, [23] N-confused porphyrin,[24] BODIPY[25] or corroles[26] have been successfully used for making D-A systems. Of these, we are particularly interested in corrole based D-A systems.

Corrole macrocyle is a contracted analogue of a porphyrin in which one *meso* position has been eliminated, resulting in a direct pyrrole-pyrrole bond, yet possessing the 18-π electron aromaticity of porphyrins.[27] When compared with porphyrins, corroles are tribasic aromatic macrocycles exhibit interesting properties which include stabilization of unusual high oxidation states of transition metal centres, lower oxidation potentials, higher fluorescence quantum yields, larger Stokes shift, and relatively higher extinction coefficients in the red part of the optical spectrum.[28-30] A few D-A systems based on corroles have been reported in the literature to understand natural photosynthetic phenomena.[31-37] These D-A systems have been constructed by using either at *meso*-phenyl position or at the axial position of resident metal ion of corrole macrocycle. For example, our group has been utilized axial position/s of resident metal ion of corrole macrocycle, constructed hetero oligomers and studied effect of metal ion on PET and EET reactions.[31,32] Ngo et al. have constructed mixed corrole-porphyrin multichromophoric systems by using *meso* positions of macrocycle and studied singlet-singlet energy transfer process by using transient absorption spectroscopy.[34] D'Souza and co-workers have used *meso* positions of donor corrole and

[a] *Inorganic & Physical Chemistry Division, CSIR-Indian Institute of Chemical Technology, Habsiguda, Hyderabad-500007, (Telangana), India .Email: giribabu@iict.res.in. Phone: +91-40-27191724, Fax: +91-40-27160921*

[b] *Academy of Scientific and Innovative Research (AcSIR), New Delhi, India.*

[c]

† Electronic Supplementary Information (ESI) available: ^{1}H NMR and ESI-MS spectra, cyclic voltammograms, fluorescence spectra, optimized structure, frontier molecular orbitals, and transient absorption spectra] See DOI: 10.1039/x0xx00000x

constructed corrole-fullerene dyads with rate of charge separated state ~10^{10}–10^{11} s^{-1}.[34] Recently, we have utilized β-pyrrole position of corrole macrocycle and constructed corrole-polycyclic aromatic hydrocarbons (either pyrene or fluorene) dayds.[38] The excited state properties revealed that there is an energy transfer from polycyclic aromatic hydrocarbon to corrole macrocycle. During the course of our research in the construction of D-A systems by using β-pyrrole position of corrole macrocycle, here we reported synthesis, characterization and photophysical properties of corrole-anthraquinone, (**Cor-AQ**) and corrole-ferrocene, (**Cor-Fc**) conjugates (Figure 1). Ferrocene is a stable aromatic sandwich organometallic compound and numerous porphyrin-ferrocene conjugates have been reported in literature, in which a photoinduced electron transfer takes place from ferrocene to excited state of porphyrin.[39,40] In contrast, quinone is ultimate electron acceptor during natural photosynthesis resulting in a long-lived, charge-separated state and substantial number of porphyrin-quinone systems has been reported in literature for mimicking photosynthesis.[9] Both the dyad systems (**Cor-AQ** & **Cor-Fc**) have been completely characterized by elemental analyses, MALDI-MS, UV-Visible, ^{1}H NMR and fluorescence (steady-state and time-resolved) spectroscopies as well as electrochemical methods. In addition, we compared the photophysical properties of corrole-ferrocene and corrole-anthraquinone dyads for first time to the best of our knowledge.

Experimental Section

Materials

Commercially available reagents and chemicals were used in the present investigations. Analytical reagent grade solvents were used for synthesis, and distilled laboratory grade solvents were used for column chromatography. Dry chloroform and dichloromethane were prepared by argon-degassed solvent through activated alumina columns. Nitrogen gas (oxygen-free) was passed through a KOH drying column to remove moisture. Neutral Alumina (mesh 60-325, Brockmann activity1) was used for column purification. All the reactions were carried out under nitrogen or argon atmosphere using dry degassed solvents and the apparatus was shielded from ambient light.

Synthesis

5,10,15-tri tolyl corrole (**TTC**), and corrole phosphonium salt (**TTC-CH_2-$PPh_3^+Br^-$**) were synthesized according to reported procedures.[38,41]

Synthesis of Corrole-Ferrocene dyad (Cor-Fc). Ferrocene-2-carboxaldehyde (12 mg, 0.055mmol), 18-Crown-6 (10 mg, 0.04 mmol), anhydrous potassium carbonate (15 mg, 0.1 mmol) and corrole phosphonium salt TTC-CH_2-PPh_3+Br^- (50 mg, 0.055 mmol) were dissolved in 6 ml of dry DMF. The reaction mixture stirred at room temperature for 4 h under nitrogen atmosphere. Solvent removed under reduced pressure, washed with water, and dried under vacuum. The obtained solid material subjected to silica gel column chromatography and eluted with $CHCl_3$:Hexane (50:50 v/v) mixture. The solvent front running brown color band was collected and recrystallized from $CHCl_3$:Hexane to get the desired product in 65% yield. Anal. Calcd. for $C_{52}H_{42}FeN_4$ % (778.70): C, 80.20; H, 5.44; N, 7.19. Found C, 80.25; H, 5.40; N, 7.25. ESI-MS: m/z = 780 (M^++2H). ^{1}H-NMR(500 MHz,$CDCl_3$,TMS) δ(PPM): -2.85(s,3H), 2.66(s,6H), 2.77(s,3H), 4.16(s,5H), 4.26(d,4H), 6.78(d,1H), 7.49-7.7(m,7H), 7.97-8.23(m,12H), 8.92(d,1H).

Synthesis of 4-(9,10-dihydro-9,10-dioxoanthracen-6-yl)benzaldehyde (AQ-CHO). This compound was synthesized slightly modified literature procedure.[42] 2-bromoanthracene-9,10-dione (50 mg, 0.174 mmol), (4-formylphenyl)boronic acid (30 mg, 0.209 mmol) was dissolved in 12 ml of dry DMF. To this 3 ml of 2M Na_2CO_3 solution was added and the reaction mixture degassed for 30 min. $Pd(PPh_3)_4$ (5 mg, 0.0174 mmol) added to reaction mixture and refluxed for 18 h under nitrogen atmosphere. Reaction monitored through TLC. After completion of reaction, the compound extracted with dichloromethane, organic layer separated, dried and residue was purified by column chromatography using silica gel with an eluent of ethylacetate:Hexane (2:8, v/v) to get the desired compound as yellow solid (yield,70%). Anal. Calcd. for $C_{21}H_{12}O_3$ % (312.3): C, 80.76; H, 3.87; N, 15.37. Found C, 80.75; H, 3.90; N, 15.35. ESI-MS: m/z=311 (M^++H). ^{1}H-NMR (500 MHz, $CDCl_3$, TMS) δ(PPM): 7.83-7.93(dd,4H), 8.09(dd,3H), 8.34-8.45(dd,3H), 8.59(s,1H), 10.1(s,1H).

Synthesis of Corrole-Anthraquinone Dyad (Cor-AQ). We have adopted similar procedure for the synthesis of Cor-Fer to this compound. The only the difference is that, we have used 4-(9,10-dihydro-9,10-dioxoanthracen-6-yl)benzaldehyde instead of ferrocene-2-carboxaldehyde. (yield, 75%). Anal. Calcd. for $C_{62}H_{46}N_4O_2$ % (877): C, 84.91; H, 5.06; N, 6.39. Found C, 84.95; H, 5.00; N, 6.35. ESI-MS: m/z =877 (M^++H). ^{1}H-NMR(500 MHz,$CDCl_3$,TMS) δ(PPM): -2.88 (s, 3H), 2.67 (s, 6H), 2.79 (s, 3H), 7.34 (dd,1H), 7.41-7.75 (m,12H), 7.96-8.84 (m, 20H), 8.93(s, 1H).

Methods and Instrumentation

^{1}H NMR spectra were recorded on a 500MHz INOVA spectrometer. Cyclic and differential-pulse voltammetric measurements were performed on a PC-controlled electrochemical analyzer (CH instruments model CHI620C). All these experiments were performed with 1 mM concentration of compounds in dichloromethane at a scan rate of 100 mV s^{-1} in which tetrabutyl ammonium perchlorate (TBAP) is used as a supporting electrolyte as documented in our previous reports.[43] The optical thin layer electrochemical studies were carried on Maya 2000 Ocean Optics software using DT-MINI-2-GS, UV-VIS-NIR LIGHTSOURCE.

Theoretical Calculations

Full geometry optimization computations of the **Cor-Fc** and **Cor-AQ** dyads were carried out with the DFT-B3LYP method using 6-31G* basis set and frequency analysis confirmed that the obtained geometries are to be genuine global minimum

structures. All calculations were performed with the Gaussian G03 (d01) package on a personal computer.[44]

Steady State Absorption and fluorescence measurements: The optical absorption spectra were recorded on a Shimadzu (Model UV-3600) spectrophotometer. Concentrations of solutions are ca. to be 1 x 10^{-6} M (corrole Soret band) and 5 x 10^{-5} M (corrole Q-bands). Steady-state fluorescence spectra were recorded on a Fluorolog-3 spectrofluorometer (Spex model, Jobin Yvon) for solutions with optical density at the wavelength of excitation (λ_{ex}) ≈0.05. Fluorescence quantum yields (ϕ) were estimated by integrating the fluorescence bands and by using 5,10,15-triphenyl corrole (ϕ = 0.21 in toluene), as reference compounds.[29]

Fluorescence Up-Conversion / Fluorescence Optical Gate: Detail description of our femtosecond laser apparatus was described elsewhere.[45] However, in brief, for fluorescence up-conversion study FOG 100-DX system (CDP System Corp. Moscow, Russian Federation) was used. Fundamental laser output (~500 mW at 800 nm) of Ti:sapphire oscillator (Mai Tai HP, Spectra Physics) was steered into CDP2015 frequency conversion unit forming the second harmonic (SH). A beam splitter (BS) is used to split the input beam (SH of fundamental) to excitation and gate (fundamental residual pulses) beams. The excitation beam directed to a rotating sample cell with the help of six mirrors and one BS. A lens (f=40 mm) was used to focus excitation beam into the sample. A neutral density (ND) filter was used for the excitation attenuation. The gate beam was directed by two mirrors to gold-coated retro- reflector mirror connected to 8 ns optical delay line before being focused together with the fluorescence (collected by an achromatic doublet, f=80 mm) on 0.5 mm type-I BBO crystal. The angle of the crystal was adjusted to phase matching conditions at the fluorescence wavelength of interest. The up-converted signal (in the UV range) was focused with a lens (f=60 nm) to an input slit of the monochromator (CDP2022D). The intensity of the up-converted radiation was measured with a photomultiplier tube operating in the photon counting mode. Proper filters were used before the detector to eliminate parasitic light from the up-converted signal if any. The polarization of the excitation pulses was set at magic angle relative to that of the gate pulses. using Berek's variable wave plate. The sample solutions were placed in a 0.6 mm or 1 mm rotating cell and absorbance of about ~0.6 at excitation wavelength generally used (yielding a concentration around 100-200 μM). The FWHM of the instrument response function (IRF) in this setup was calculated about 240 fs in the 0.4 mm cell and 280 fs in the 1 mm cell. Hence, a time resolution of <200 fs could be achieved. For data analysis, the fluorescence time profile at a given emission wavelength I(λ,t) was reproduced by the convolution of a Gaussian IRF with a sum of exponential trial function representing the pure sample dynamics S(t). Gaussian term was added to account for fast non-exponential processes if any owing to vibrational or other solvent relaxation process.

Femtosecond Transient Absorption/pump-probe: Transient absorption studies were performed using pump-probe set up of

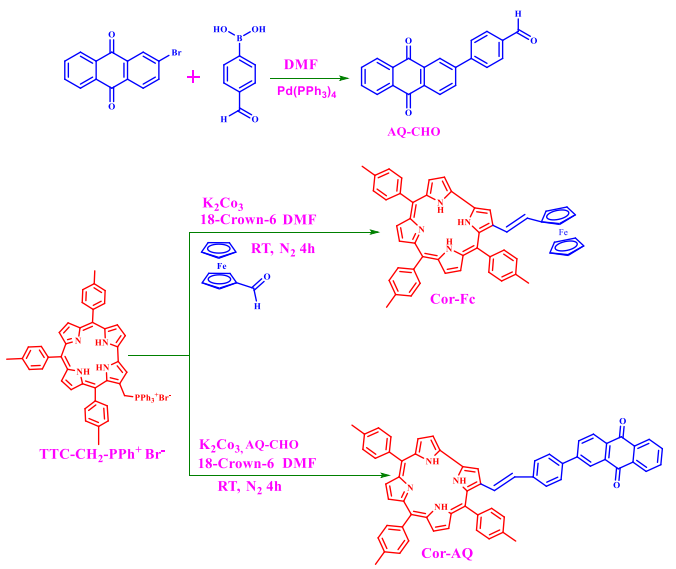

Fig 1. Synthetic scheme of **Cor-Fc** and **Cor-AQ** dyads

CDP Systems Corporation, ExciPro. The output of optical parametric amplifier (TOPAS prime) was used as pump sources at required wavelength and feed into spectrometer through synchronized chopper for 1 kHz repetition rate. A lens (f=200mm) was used to adjust the pump diameter while an iris and neutral density filter combination were used to adjust the pump energy. A Berek's variable wave plate was placed in the pump beam and polarization was fixed at magic angle with respect probe pulse. A part of the output of Ti:sapphire regenerative amplifier (Spitfire Ace, Spectra Physics) with 1 kHz repetition rate and ~100mW average power at 800 nm was fed to the spectrometer. The power of the 800 nm was reduced to 20-25 mW and focused onto a thin rotating (2-mm) CaF_2 crystal window to generate a white-light continuum. A fraction of this beam was sent to a photodetector which controls speed and phase of the chopper rotation. The beam of white light was collimated with parabolic mirror (f=50 mm, 9^0 deg). Then this white light was reflected from a beam splitter and mirror into two identical probe and reference beams. Two concave mirrors (f=150 mm) were used to focus both probe and reference beams to the rotating sample cell. Two lenses (f=60 mm) made probe and reference images at the entrance surfaces of two optical fibers which are connected to the entrance slit of the imaging spectrometer (CDP2022i). This spectrometer consists of UV-Vis photodiode (Si linear photodiode) arrays and IR Photodiode (GaAS linear photodiode) array with spectral response range 200-1000 nm and 900-1700 nm respectively. Quartz cells of 1 mm sample path length were used for all studies and IRF was estimated to be ≤150 fs. For sub ps dynamic, signal from solvents system was recorded under same experimental conditions and placed in respective figures in the text for comparison where overlapping of solvent induced transient with transient signal from sample is substantial. However, to minimize the solvent signal pump pulse energy was kept below 3 μJ per sec and probe pulse energy was from 0.1-0.5μJ at the sample. For transient absorption spectra the group velocity

dispersion compensation of white light continuum (probe beam) was done using studied solvent's two photon absorption data for few ps delay. All the samples were checked before and after taking the transient absorption to monitor the sample degradation if any.

Results and Discussions

Synthesis

Synthetic scheme for preparing both the dyads are shown in Figure 1. 4-(9,10-dihydro-9,10-dioxoanthracen-6-yl)benzaldehyde (AQ-CHO) was achieved by condensation of 2-bromoanthraquinone with (4-formylphenyl)boronic acid. The starting material corrole phosphonium salt (TTC-CH_2-$PPh_3^+Br^-$) was synthesized according to the literature.[38] Both the dyads were synthesized by using Wittig-Horner reaction to create conjugation (double bond) between the β-pyrrole position of the corrole and either ferrocene or anthraquinone moeities.[46] Finally, the crude compound was purified by chromatography using a flash silica gel column. Both the dyads were found to be stable at room temperature. Preliminary characterization of the both dyads was carried out by ESI-MS and UV-Visible spectroscopic methods. The mass spectrum of both the dyads **Cor-Fc** and **Cor-AQ** showed peaks at m/z = 780 ($[M]^+$+H, $C_{52}H_{42}FeN_4$) and 877 ($[M]^+$, $C_{62}H_{46}N_4O_2$) respectively, are ascribable to the molecular-ion peak (*S1 & S2 Supporting Information*).

^{1}H-NMR spectral data of both the dyads have been summarized in the experimental section and the spectra of **Cor-Fc** and **Cor-AQ** are shown Figure S3. Comparison of these spectra with those of individual constituents (**TTC**, **Fc-CHO** and **AQ-CHO**) reveals that there are certain specific changes in peak positions of various protons present on corrole macrocycle and that of its individual constituents. For example, the tolyl protons of corrole macrocycle split into two singlets in **Cor-Fc**. The singlet and doublet at 4.16 & 4.26 ppm, respectively, are belongs to ferrocene protons. The two doublets appeared at 6.50 and 7.25 ppm are belongs to vinylic protons. This further confirms the formation of dyads. A similar set of peaks were observed in Cor-AQ dyad.

Ground State Properties

The electronic absorption spectra of the dyads **Cor-Fc** along with their constituent monomers in CH_2Cl_2 solvent are shown in Figure 2. The wavelength of absorption maxima and molar extinction coefficients along with monomeric units are listed in Table 1. The monomeric component **Fc-CHO** shows a band at 220 nm due to $Fe(a_{1g})\rightarrow Cp(e_{1g})$ charge transfer whereas peak at 450 nm region due to symmetry forbidden $Fe(a_{1g})\rightarrow Fe(e_{1g})$ transitions (Figure 2). In contrast, the monomeric component **AQ-CHO** shows a series of bands between 220 and 330 nm due to π-π* transitions (see *supporting information*). As shown in Figure 2, the absorption

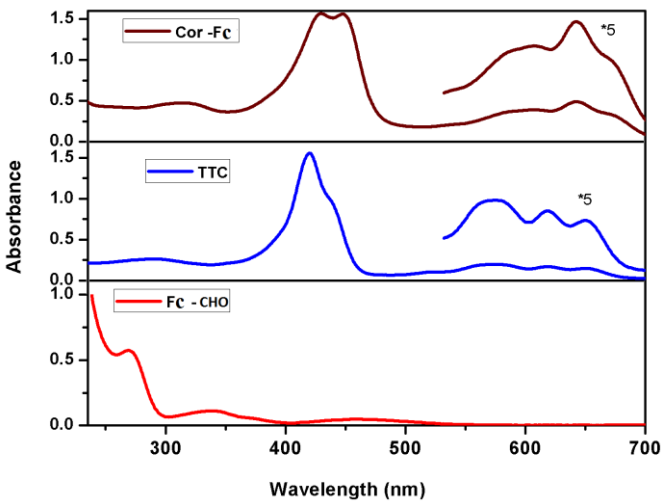

Fig. 2. Absorption behaviour of **TTC**, **Fc-CHO**, & Cor-Fc in CH_2Cl_2 using 0.01 mM concetration.

Table 1. Absorption and Electrochemical data.

	Absorption, λ_{max}, nm (log ε, M^{-1} cm^{-1})[a]		Potential V vs SCE[b]	
compound	**corrole-bands**	**metallocene /quinone Bands**	**oxidation**	**reduction**
TTC	417(5.33), 572(4.39) 617(4.33), 650(4.27)	-	0.57, 0.84, 1.26, 1.80	-0.52, -1.74
AQ-CHO	-	283(4.32), 340(3.65).	-	-0.96, -1.38
Fc-CHO	-	269(3.59), 338(2.87), 460(2.5).	0.48	-
Cor-Fc	444(4.49), 426(4.50) 606(3.83), 642(3.93) 675(3.73).	260(3.95), 310(3.91)	0.69, 0.90, 1.25, 1.69	-0.60, -1.40
Cor-AQ	426(4.48), 448(4.45) 606(3.89), 639(3.95) 668 (3.80)	255 (4.16), 302 (4.10)	0.58, 0.81 1.24, 1.77	-0.59, -1.04 -1.53

[a]Solvent CH_2Cl_2. Error limits: λ_{max}, ±1 nm; log ε, ±10%. [b]CH_2Cl_2, 0.1 M TBAP. Glassy carbon working electrode; standard calomel electrode is reference electrode, Pt electrode is auxiliary electrode. Error limits, $E_{1/2}$ ± 0.03 V.

spectra of the dyad merely superposition of the absorption spectra of monomer Ferrocene and corrole and it is dominated by corrole $S_0\leftarrow S_1$ (Q-band) and $S_0\leftarrow S_2$(Soret band) transitions due to their high molar extinction coefficient. Introduction of ferrocene or anthraquinone at the β-pyrrole position of corrole results in the following changes of the absorption spectra: (a) a red-shift along with broadening and splitting of the Soret band (~10 nm); (b) a red-

shift of the Q bands (~25 nm). The split in Soret band and red-shift withdrawing bulky substituents at β-pyrrole of corrole of corrole absorption bands are probably due to the electron macrocycle, which devaiate the planarity of the corrole macrocycle.[35] On the other hand Gryko et al. did not observer any π-π interactions when a ferrocene attached at *meso* position of a corrole.[47] The broadening is more pronounced at the longer wavelength region (>600 nm) (Figure S4 *supporting information*) which might be due to the presence of donor-acceptor type of molecular arrangement which promotes charge delocalization and thus leads to ground state stabilization. In contrast, broadening can also be due to many conformers at different orientations of corrole units around the two –C=C– bonds. The observations of broadening, red-shift and split in the Soret band suggest a modest electronic interaction between the corrole π-system and the substituents either ferrocene or anthraquinone. Such kind changes were not observed when absorption spectra taken in 1:1 equivalent mixture solution of corrole and ferrocene or anthaquinone (*see* Figure S5).

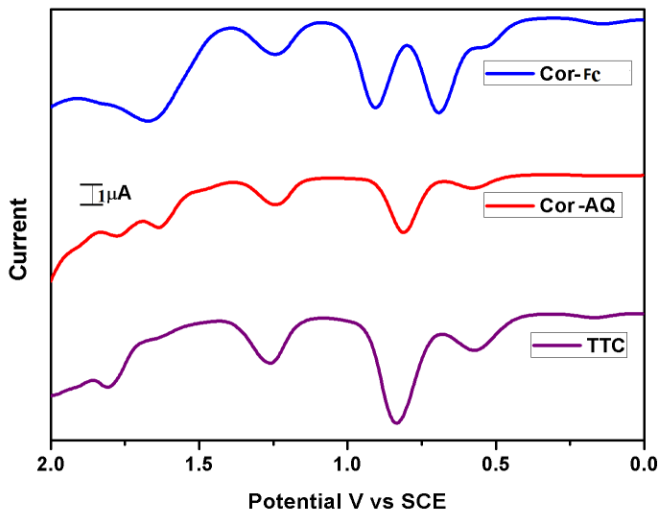

Fig. 3. Differential pulse voltammograms of **Cor-Fc**, **Cor-AQ** and **TTC** in CH_2Cl_2 with 0.1M TBAP.

With a view to evaluate energies of the charge separation states (E_{CS}), which, as will be discussed in a later part of this paper, are useful quantities in analyzing the photochemical properties of these dyads, we have carried out electrochemical investigation using differential pulse voltammetric technique. Figure 3 depicts the differential pulse voltammograms of **TTC**, **Cor-Fc** and **Cor-AQ**. Table 1 summarises the redox potential data (CH_2Cl_2 and 0.1 M TBAP) of the D-A systems investigated in this study along with that of the corresponding individual constituents. From the Figure 3 and Table 1, both the dyads investigated under same experimental conditions show four oxidations and three reduction peaks. Wave analysis suggested that, while the first two reduction steps in **Cor-AQ** and first two oxidation steps in **Cor-Fc** are reversible (i_{pc}/i_{pa} = 60−70 mV; ΔE_p = 65 ± 3 mV for ferrocenium/ferrocene couple) reactions, the subsequent steps are, in general, either quasi-reversible ($E_{pa} - E_{pc}$ = 90−200 mV and i_{pc}/i_{pa} = 0.5−0.8 in the scan rate (ν) range 100−500 mV s^{-1}) or totally irreversible. Figure 4 and Table 1 also reveals that the electrochemical redox potentials of the both the dyads are slightly shifted as those of their corresponding monomeric analogues. For instance, the first reduction peak of **Cor-AQ** at -0.59 V is belongs to corrole part of the dyad whereas the second reduction at -1.04 is belongs to the anthraquinone part of the dyad as in case of their monomeric units it appeared at -0.52 and -0.96 V for corrole and anthraquinone, respectively.

To distinguish the redox potentials of these dyads spectroelectrochemistry was carried out under same solution conditions as per differential pulse voltammetry measurements. Upon the first controlled potential reduction of **Cor-AQ** at -0.70 V, the Soret band at 426 nm decreases its intensity with red-shifted to 446 nm as shown in Figure 4 while Q band at 637 nm also red-shifted to 678 nm with increasing intensity. During this process isosbestic points were observed at 313, 355, 523 647 nm. The intensity of newly formed band at 678 nm further increases its intensity upon the third controlled reduction potential at -1.70 V. The step-wise reduction products are assigned as π-anion and dianion radical.[48] No spectral changes were observed when controlled reduction potential at -1.30 V. This is probably due to the reduction of anthraquinone at this potential. The spectral changes obtained during first and second oxidations are illustrated in Figure 4. Upon controlled oxidation potential at 0.70 V, the Soret band at 423 nm decreases its intensity with red-shift to 465 nm. Whereas Q band at 635 nm decreases its intensity with formation a new band at 714 nm. During this process isosbestic points are observed at 469 and 684 nm. The new band at 714 nm further increases its intensity when controlled potential is shifted to 1.05 V. Similar spectra have been assigned to corrole cation radicals, and a π-cation radical assigned to the present study.[49] We have not observe any oxidation wave of (AQ) under the experimental conditions employed. Therefore the oxidation waves are belongs to purely corrole part of **Cor-AQ** dyad.

Spectral changes of **Cor-Fc** upon controlled reduction potential at -1.75 V illustrated in Figure 5. The Soret band at 423 nm was red-shifted to 437 nm with change in intensity of the band. Whereas the Q band at 640 nm decreases its intensity with the formation of new band at 668 nm. During this process isosbestic points were observed at 456, 518 and 648 nm. The reduction product was assigned as π-anion radical as there was no reduction observed in Ferrocene. When the controlled potential shifted to 0.75 V, the Soret band decreases its intensity and red-shifted to 431 nm, while intensity of Q band at 642 nm reduces intensity with formation new band at 715 nm. The intensity of newly formed band then decreases upon second controlled potential oxidation at 1.10 V. The step-wise oxidation products are assigned as π-cation radical and dication.

Theoretical Calculations

In order to examine the nature and position of frontier molecular orbital's, density functional theory (DFT) calculations have been carried.[44] Complete optimization without any constraint was done using B3LYP and 6-31g(d) basis set to see the structural parameters of the two systems, **Cor-Fc** and **Cor-AQ**. Figure 6 displays the HOMO and LUMO distribution and geometrical optimized structures of the dyads obtained by DFT calculations. From Figure 6, it is clear that the HOMO is mainly distributed at corrole moiety while LUMO mainly distributed at anthraquinone moiety in **Cor-**

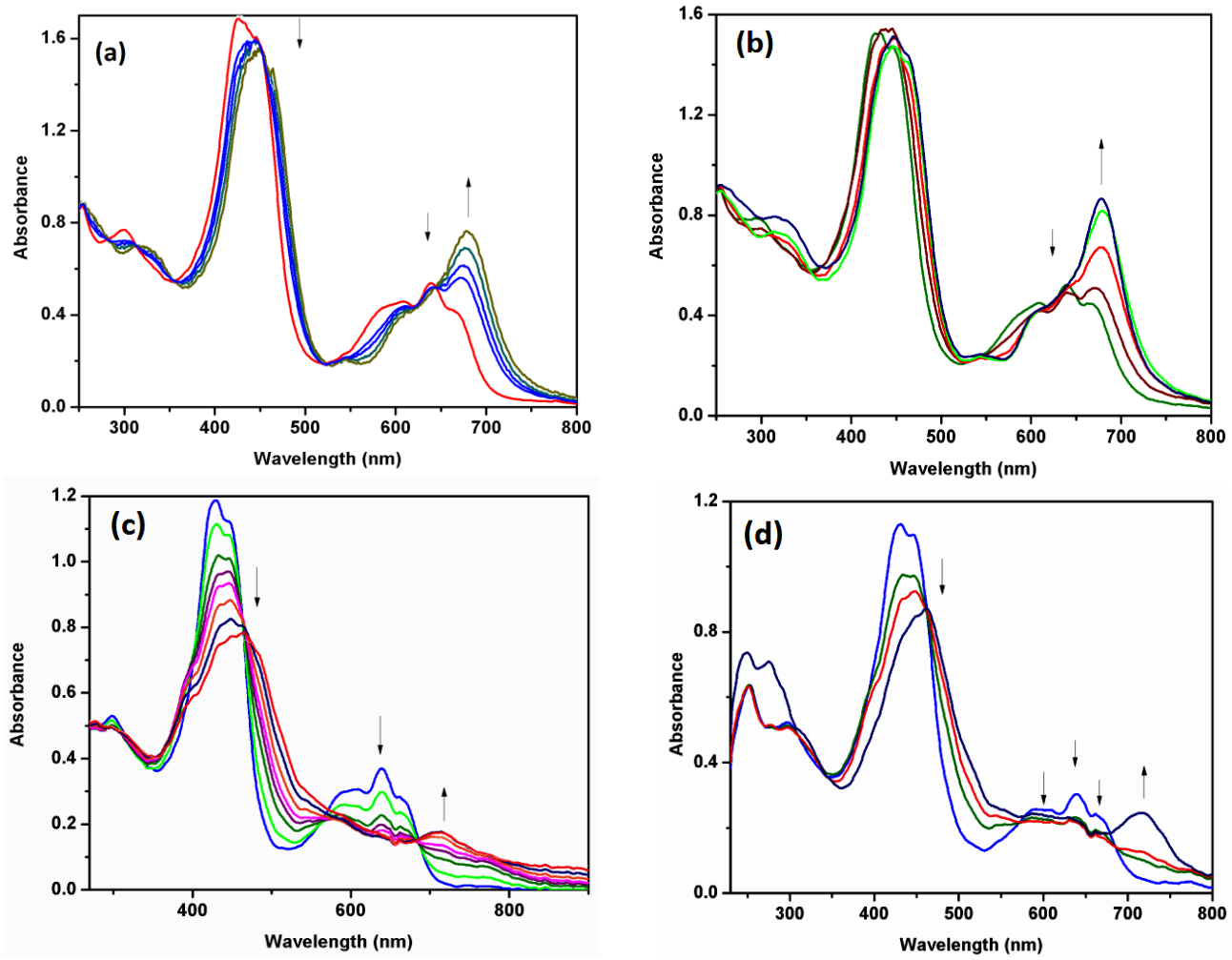

Figure 4. In-situ UV-Visible spectroelectrochemical changes of (**Cor-AQ**) at applied redox potential (a) -0.70 V (b) -1.70 V (c) +0.70 V and (d) +1.05 V, using SCE as reference electrode.

AQ. Whereas in **Cor-Fer**, the HOMO-1 is distributed among corrole and ferrocene moieties of the dyad and LUMO is distributed mainly on corrole (Figure 6). The energies of HOMO and LUMO for dyads **Cor-AQ** and **Cor-Fc** were found to be -4.56 & -4.85 eV and -2.71 & -2.15 eV, respectively. From the geometrical optimized structures (Figures S10 and S11 *Supporting Information*), in both the dyads the corrole macrocycle and either anthraquinone or ferrocene are far apart. Moreover, phenyl rings at *-meso* positions are found to be perpendicular to the plane of corrole ring, which prevent the stacking interaction. All these observations corroborate the prevalence of *through-bond* intramolecular electron transfer mechanism in the current systems.

Singlet State Properties

Unlike the case with the ground state properties, major differences have been noticed in the singlet state properties of both the dyads. Steady-state fluorescence emission spectra of both the dyads have been measured in four different solvents (hexane, dichloromethane, acetonitrile and DMF) with change of polarity and compared with constituent fluorescence emission spectra of **TTC** in corresponding solvent as shown in Figure 7. The corresponding singlet state data were presented in Table 2. The fluorescence emission maxima (λ_{em}) of both the dyads are red-shifted, when compared to its reference compound TTC in all investigated solvents (λ_{ex} = 425 nm). A similar kind of red-shifted fluorescence emission behaviour was also observed in other β-pyrrole substituted corroles.28 The red-shift of the fluorescence emission spectra of both dyads are presumably due to increased polarity of the emitting state

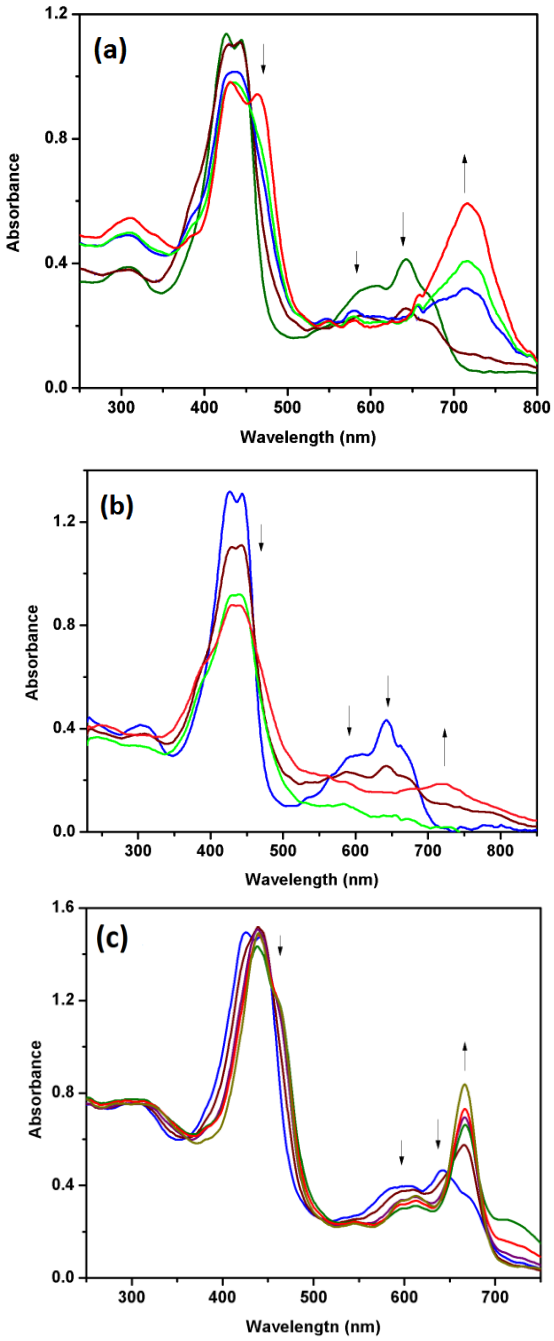

Fig. 5. In-situ UV-Visible spectroelectrochemical changes of **Cor-Fc** at applied redox potential (a) +0.75 V (b) +1.1 V and (c) -1.75 V, using SCE as reference electrode.

originated from the donor-acceptor (D-A) type of molecular arrangement. Interestingly, we observe remarkable quench in corrole emission intensity when equi-absorbing solutions of dyads were excited at 425 nm (λ_{max}, where corrole absorbs predominantly). The possibility of self-aggregation of corroles which leads to quenching of fluorescence intensity (as a result of non radiative path in the excited state) can be ruled out as all experiments were carried out with very dilute solutions (10^{-6} M). Moreover, we could not observe substantial changes in the absorption spectra as it happens in few corrole systems.

Various radiative and non-radiative intramolecular processes can be conceived to participate in the excited state decay of **Cor-Fc** & **Cor-AQ**. Among these, an excitation energy transfer (EET) or photoinduced electron transfer (PET) can be assumed to participate in the quenching of fluorescence emission intensity. For EET, the emission spectrum of donor has to be overlapped with absorption of the acceptor. It is evident from the Figures 2 & 7 that the EET is not possible between corrole and either anthraquinone or ferrocene due to lack of proper spectral overlap. Alternative pathway for emission quenching is the intramolecular PET. The E_{00} (0-0 spectroscopic transition energy) values of corrole part of dyads, 1.89 ± 0.05 eV, 1.90 ± 0.05 eV for **Cor-Fc** and **Cor-AQ**, respectively as estimated from overlap of their absorption and emission spectra were found to be in the same range as the E0-0 values of free TTC.[38] When excited at 425 nm, the singlet excited state of corrole either can donate an electron to an energetically favourable acceptor (Oxidative electron transfer) or can take an electron from a suitable donor (reductive electron transfer). The change in free energy for PET from the corrole to the anthraquinone in **Cor-AQ** can be calculated using the equation 1.

$$\Delta G^0(1Cor \rightarrow AQ) = e[E(Cor^*/Cor^{\cdot+}) - E(AQ/AQ^{\cdot-}) - E_{00}(Cor) \quad (1)$$

ΔG^0 was found to be -0.73 eV when excited at 425 nm. Whereas in case of **Cor-Fc**, the change in free energy for a PET reaction from ground state of ferrocene to singlet state of corroles was found to be -0.60 eV. A PET reaction from singlet state of corrole to ground state of ferrocene thermodynamically is not feasible (ΔG^0 was found to be 0.59 eV).

Fluorescence quantum yields of the dyads and individual constituent have been estimated (Table 2) by comparing the emission spectra of reference compound (i.e., TTC (ϕ) = 0.21 in toluene) with that of the dyads.[29] It was found that the fluorescence quantum yield (ϕ) of **Cor-Fc** and **Cor-AQ** was 0.012 and 0.013, respectively in CH2Cl2. The fluorescence quenching efficiency (Q) of the dyads was calculated by equation 2.

$$Q = \frac{\emptyset_{TTC} - \emptyset_{Dyad}}{\emptyset_{TTC}} \quad (2)$$

Where $\emptyset_{TTC}$ refer to the fluorescence quantum yields for tritolyl corrole and $\emptyset_{Dyad}$ refer to (**Cor-Fc**) or (**Cor-AQ**); (λex = 425 nm). As the static dielectric constant of the solvent is increased, the quenching of fluorescence intensity increased gradually (Table 2), indicate the excited state electron transfer mechanism. For example, quenching efficiencies in hexane are less compared to the CH_2Cl_2, CH_3CN and DMF. In general, the PET process is accelerated in polar solvents than the non-polar solvents, so the present results are in consistent with the literature.[39] In all investigated solvents, the efficient quenching of the dyad **Cor-AQ** relative to that of the **Cor- Fc** can be directly attributed to the more exothermic value of ΔG_{PET} of **Cor-AQ**.

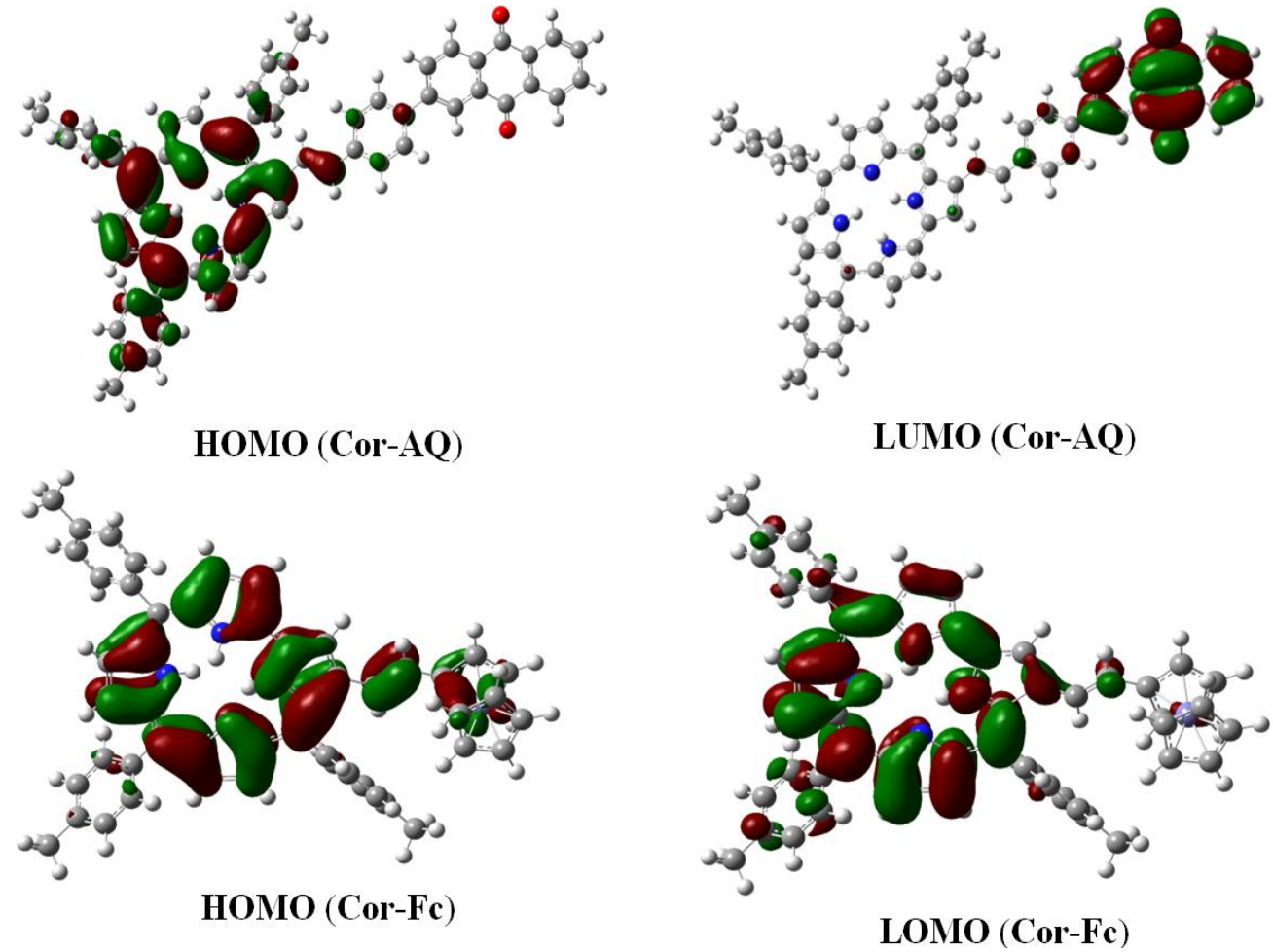

Fig. 6. HOMO-LUMO of **Cor-AQ** (above), HOMO-LUMO of **Cor-Fer** (below).

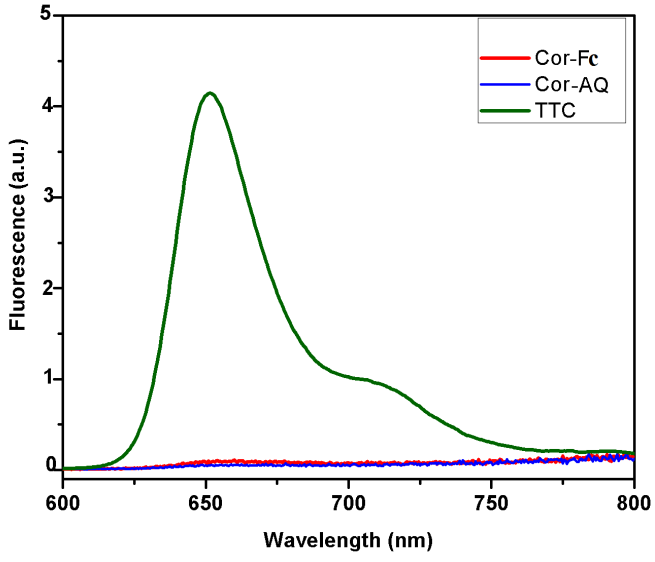

Fig. 7. Fluorescence spectra of **Cor-Fc**, **Cor-AQ** and **TTC** at λ_{ex} = 425 nm in acetonitrile of equi-absorbing solutions (O.D. λ_{ex} = 0.05).

Table 2. Steady state emission data

	λ_{em}, nm[a] (ϕ, %Q)[b], λ_{ex} = 425 nm			
Compound	**Hexane**	**CH_2Cl_2**	**CH_3CN**	**DMF**
TTC	671 (0.29)	674 (0.25)	651 (0.24)	655 (0.29)
Cor-Fc	688 (0.012, 95)	690 (0.012, 95)	663 (0.014, 94)	668 (0.012, 96)
Cor-AQ	680 (0.13, 95)	683 (0.013, 95)	656 (0.012, 95)	664 (0.01, 97)

[a]Error limits: λ_{ex}, ±2 nm, ϕ ± 10%. [b]Q is defined in equation 2 (see text).

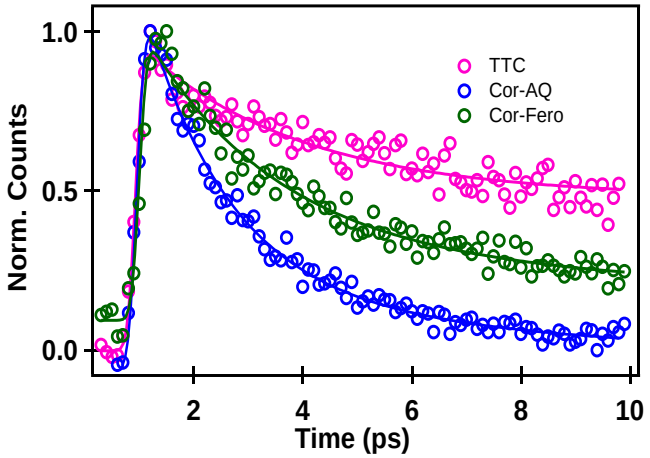

Fig. 8. Time profile of fluorescence up-conversion signal of **TTC**, **Cor-AQ**, and **Cor-Fc** dyads upon 410 nm excitations in acetonitrile solvent.

Table 3. Kinetic parameters of fluorescence Up-conversion data analysis.

Signal	λ_{Probe} (nm)	1st Component τ_1(ps), A_1	2nd Component τ_2 (ps), A_2	3rd component (τ_3≡3.5 ns),A_3	CS (ps)
TTC	670	3, 47%	----	53%	----
Cor- AQ	670	2±0.5, 98%	-----	2%	2
Cor-Fc	670	2.5 ±0.2, 85%	355±90, 9%	6%	36 [a]

[a]Weighted average of 1st and 2nd component($\tau_{avg} = \frac{(\tau_1 \times A_1 + \tau_2 \times A_2)}{(A_1 + A_2)}$)

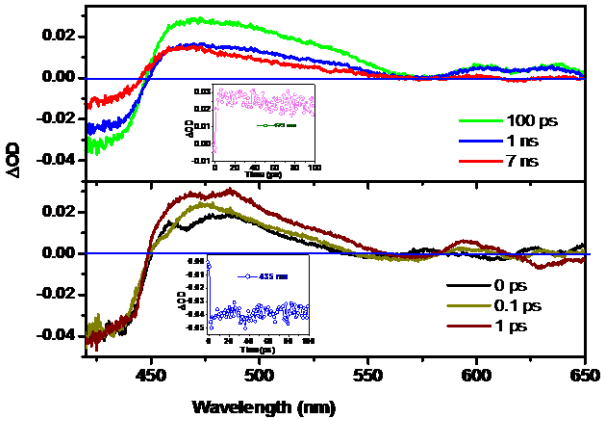

Fig. 9. Transient absorption spectra measured at several time delays after $S_2 \leftarrow S_0$ excitation at 410 nm of **TTC** in ACN. Inset shows the decay profiles of TA at respective wavelengths.

Femtosecond Time Resolved Fluorescence

Further evidence of the intramolecular PET process has been determined by measuring the excited state decay curves. The fluorescence decay of the **TTC** in ACN measured by TCSPC and is found to be monoexponential with a 3.5 ns lifetime.[29] On the other hand, the fluorescence dynamics of the dyads was observed to be too fast to properly resolved by TCSPC in any of the solvents studied and was thus measured by femtosecond time-resolved fluorescence up-conversion (FU) technique. However, to compare the extent of singlet-state quenching of corrole in the dyads, fluorescence decay was measured for **TTC**, **Cor-Fc** and **Cor-AQ** in ACN in 10 ps time window. Figure 8 shows the FU time profiles of **TTC**, **Cor -Fc** and **Cor-AQ** in ACN at 670 nm upon 410 nm excitation. The FU signal profile of **TTC** at 670 nm exhibits a biphasic decay and is well fit with 3 ps and a lifetime that is too long to be measured exactly using this equipment but is consistent to the lifetime of S1 state of **TTC** 3.5 ns. The fit curve is shown in Figure 8 and corresponding amplitudes are listed in Table 3. In analogy to the ultrafast dynamic of tetrapyrrolic systems reported elsewhere [45,50,51] the first component can be assigned to the vibrational cooling processes. However, FU signal profile of the **Cor-AQ** dyad shows very fast decay and it is nicely fit by bi-exponential components with 2 ps lifetime, a major component, along with a very weak and long 3 ns lifetime which was kept as constrained. The 2 ps component for this dyad is assigned to be due to charge separation (CS) resulting from electron transfer from singlet excited state of corrole to anthraquinone part of the dyad. Figure 8 also shows the FU signal profile of **Cor-Fc** dyad and it can be analysed with three-exponential decay components and the lifetime values of first two components were found to be 2.5 ps, 355 ps where as lifetime of the third component was kept constant at 3 ns, lifetime of free **TTC**. As shown in Table 3, 95% of decay processes are covered by first two components and the third component is only 5%. The weighted average of first two components was found to 36 ps and it is assigned to be charge separation (CS) time due to electron transfer from ferrocene to the singlet excited state of corrole. Quantum yield of charge separation, φCS, is calculated using equation (3) and found to be >99% for **Cor-AQ** and > 98% for **Cor-Fc** which are in good agreement to the steady state quenching data (Table 2).

$$\emptyset_{CS} = \frac{(1/\tau_{CS})_{Dyad} - (1/\tau_f)_{TTC}}{(1/\tau_f)_{TTC}} \qquad (3)$$

Further, rate constant (k_{ET}) for the charge transfer state $Cor^{-}Fc^{+\cdot}$ and $Cor^{+\cdot}$-$AQ^{-\cdot}$ has been calculated using equation (4) and accounted bellow.

$$k_{ET} = (1/\tau_f) - k \qquad (4)$$

where k is the reciprocal of the lifetime of the TTC, τ_f is the lifetime of **Cor-Fc** and **Cor-AQ**. The rate constant values for **Cor-Fc** and **Cor-AQ** was found to be 2.78 x 10^{10} and 3.33 x 10^{11} s^{-1}, respectively. Overall, the photoinduced reactions are influenced by the nature of the substituent which is connected to corrole macrocycle. Both in steady-state and excited state lifetime, the quenching was high for anthraquinone dyad than its corresponding ferrocene dyad. This might be due to the more electron withdrawing nature of anthraquinone and this is reflected in electrochemical

studies (Table 1). The observed CS is faster for **Cor-AQ** than for **Cor-Fc** in acetonitrile and it can be easily rationalized by considering the thermodynamic driving force which is 0.13 eV larger for Cor-AQ dyad. In terms of Marcus theory,[52] CS in these dyads is moderately exergonic (-0.60 to -0.73 eV) and takes place in the normal regime. As a results its rate constant increases with the driving force.

Femtosecond Time Resolved Absorption Spectra

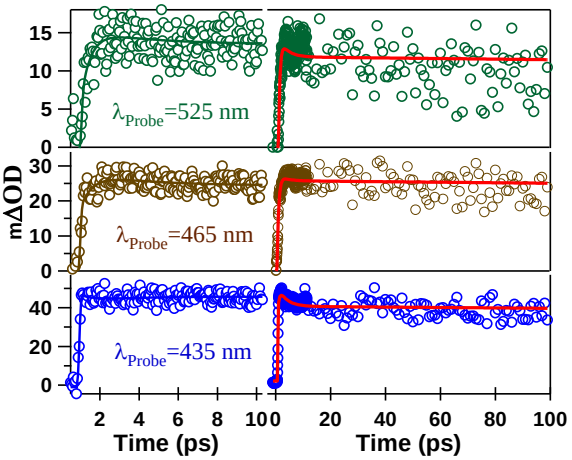

Fig. 10. Femtosecond transient absorbance of TTC in ACN. Pump wavelength was 410 nm, probe wavelengths were as shown. The ground state bleaching signal at 435 nm has been inversed to easy compare with transient absorption of singlet excited states.. Solid red lines are fits of the experimental data using a common set of lifetimes (see text). Solid lines in 10 ps data are fits to estimate ultrafast components, τ_1 and τ_2 .

Table 4. Component Relative Amplitudes of Fits of Transient Absorption Measurements for 410 and 575 nm excitation of **TTC** in ACN.

λ_{Probe} (nm)	1st Component (τ_1≡0.5±0.1 ps) A_1(%)	2nd Component (τ_2≡3±1 ps) A_2(%)	3rd Component (τ_3≡3.5 ns) A_3(%)
435	-20	25	75
	---	---	100[a]
465	-100	6	94
	---	---	100[a]
525	-100	21	79
	---	---	100[a]

[a] Amplitude correspond to the mono-exponential fit to transient absorption signal upon Q band excitation, A negative component indicates the respective component is rise instead of decay

In view to detect the radical anion/cation we have measured transient absorption (TA) spectra of TTC along with **Cor-Fc** and **Cor-AQ** in ACN upon Soret (410 nm) as well as Q band (575 nm) excitations. Figure 9 shows the typical transient absorption spectra of TTC in ACN when excited upon 410 nm (Figure S13, upon 575 nm excitation) and it is quite similar to that of well studied tetrapyrrolic system TPP.[53] The spectra exhibits two negative bands corresponding to Soret and Q band absorption centred around 420 and 560 nm and they can be assigned to the ground state bleaching (GSB) of $S_2 \leftarrow S_0$ and $S_1 \leftarrow S_0$ respectively. A strong positive signal in between 450 to 560 nm can be assigned to excited states absorption (ESA), S_n

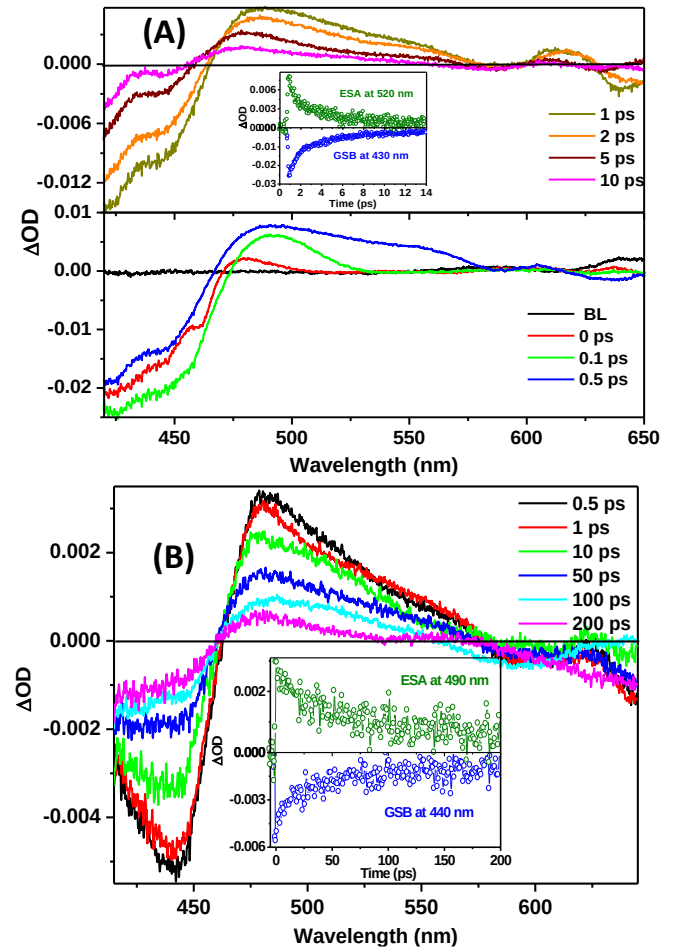

Fig. 11. Transient absorption spectra of **Cor-AQ**, λ_{ex}= 410 nm (A) and **Cor-Fc** (B) in ACN, Insets show typical excited state absorption and ground state bleaching profile of respective dyads.

$\leftarrow S_1$ transition. The dynamic features of the transient absorption was analyzed in at three different wavelengths 420, 460 and 575 nm in three different time windows of 10 ps , 100 ps and 6 ns and they are shown in Figure 10 and Figure S14&S15. The temporal evolution of all transient absorption data can be well fit with three sets of lifetime values, 0.5±0.1 ps (τ_1), 3±1 ps (τ_2) and a lifetime (τ_3) that is too long to be measured with our existing femtosecond system but this long lifetime value is very consistent with the S_1 fluorescence lifetime of 3.5 ns, measure by TCSPC method. The fit curves shown in Figure 10 where above set of lifetime values were used as constrained to fit the data. Component amplitude values are listed in Table 4. The similar sets of temporal evolution of TA signals upon 575 nm excitation were also analysed and found to be mono-exponential decay with 3.5 ns lifetime values (Figure S14). It is important to note here that $T_n \leftarrow T_1$ absorption of **TTC** is comparable to that of $S_n \leftarrow S_1$ in the wavelength range probed,[54,55] the population dynamics for equilibrated S_1 and T_1 are effectively combined in an long-lived 3.5 ns component for both S_2 & S_1 excitation for this experimental time window. These disappearances of first two components from TA signal upon Q band excitation clearly points to the fact that they are related with the ultrafast relaxation process when TTC is exited S_2. The first component

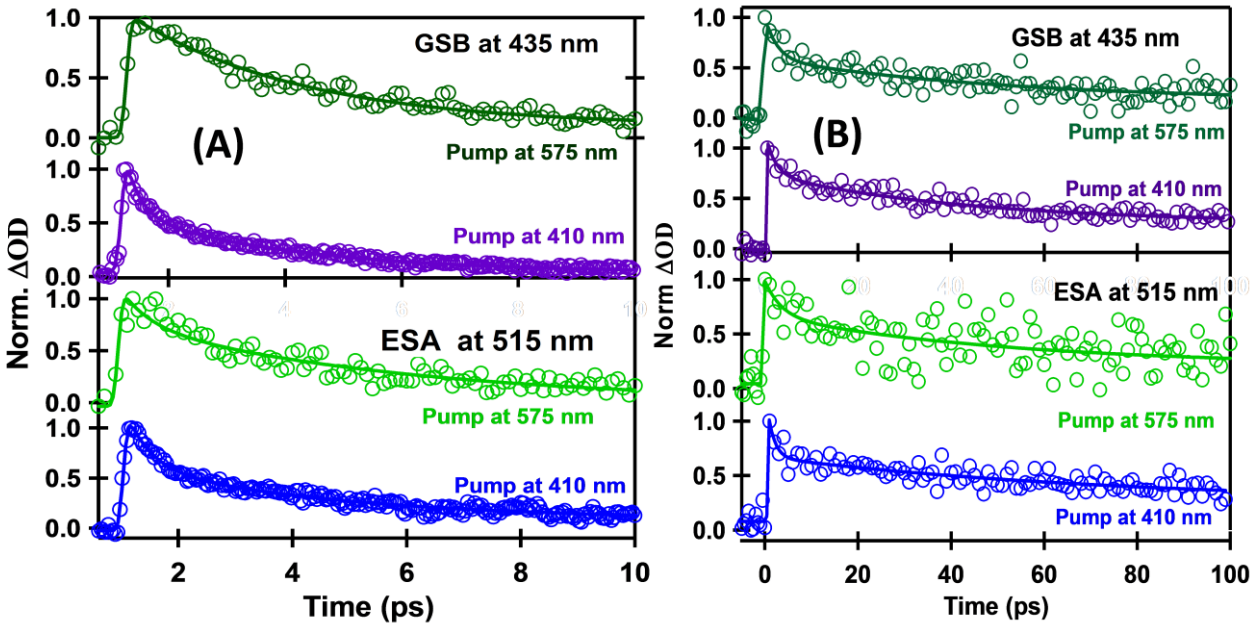

Fig. 12. Kinetic profile of excited state absorption at 515 nm (lower panel) ground state bleaching at 435 nm(upper panel) upon 410 and 575nm excitation of **Cor-AQ** (A) **Cor-Fc** (B) in ACN.

Table 5. Component relative Amplitudes of Fits of Transient Absorption Measurements for 410 and 575 nm excitation of Cor-AQ and Cor-Fc in ACN.

Dyad	Signal	λ_{Pump} (nm)	λ_{Probe} (nm)	1st comp τ_1 (ps), A_1(%)	2nd comp τ_2(ps),A_2(%)	3rd comp (τ_3≡3.5 ns),A_3(%)	CS/CR (ps)
Cor-AQ	ESA	410	515	0.5±0.05, 50	3.7± 0.3, 46	4	2 [a] (CS)
		575	515	1.9±0.1, 46	3.1± 0.1, 45	9	2.5[a] (CS)
	GSB	410	435	0.25±0.05, 48	2.9± 0.1, 49	3	1.6[a] (CR)
		575	435	------	3.0±0.1 , 94	6	3 [a] (CR)
Cor-Fc	ESA	410	515	3.5±0.2, 36	53± 2, 46	18	32[a] (CS)
		575	515	1.5±0.1, 50	73± 3, 40	10	33[a] (CS)
	GSB	410	435	2.6±0.2, 42	55± 2, 48	10	31[a] (CR)
		575	435	2.5± 0.2, 30	53±2 , 55	15	35 [a] (CR)

CS -- charge separation, CR-Charge recombination, [a] Weighted average of 1st and 2nd component ($\tau_{avg} = \frac{(\tau_1 \times A_1 + \tau_2 \times A_2)}{(A_1 + A_2)}$).

of transient decay profile of ESA signal at 465 and 525 nm upon S_2 excitation was found to be rise component with lifetime value 0.5 ps and it was found to be partially rise component in ground state bleaching signal. This ultrafast shortest component can be ascribed to $S_1 \leftarrow S_2$ internal conversion. The second and third components for both ESA and ground state bleaching signals were decay components and they correspond nicely to fluorescence up-conversion signal. Hence these components can be ascribed as vibrational cooling (3 ps) and S_1 lifetime i.e., S_1 state population decay to ground state or intersystem crossing to triplet sate (T_1) of **TTC**.

Transient absorption measured at several delays after S_2 and S_1 excitation at 410 and 575 nm respectively for both the dyads, Cor-AQ and **Cor-Fc** in ACN and they are shown in Figure 11A and 11B and Figure S16 (575 nm excitation). TA spectra for both the dyads composed of negative signals centred around 435 nm corresponding to S_2 ground state absorption and positive signal peaking around 485 nm but above 570 nm signals are too weak to be resolved. The overall shape of TA spectra for both the dyads is more or less similar to that of TTC apart from a systematic ~20 nm red shift of the peak position of transient absorption of excited states and ground state bleaching band. Interestingly, the ΔOD values of either ground state bleaching or the transient absorption of singlet excited states remarkably lower than that of TTC, when concentration of the studied systems and the pump laser power were kept similar. No distinct excitation dependent change in TA absorption spectra was observed for these two dyads. However, the intensity of TA spectra reduces to zero within 20 ps for **Cor-AQ** dyad and 200 ps for **Cor-Fc**. No distinct absorption spectra for corrole anion or corrole cation were detected but a trend of blue shift of peak position of transient absorption of singlet excited states was observed on increasing delay time. Temporal evolution of transient absorption strongly depends on probe wavelength. The transient absorption kinetics have different profiles at different wavelengths of TA spectra (Figure S17) and TA profile at around peak position is complex in nature and very difficult to fit convincingly. However, TA signal profile above 500 nm probe wavelength is quite simple and it follows the dynamic as to the fluorescence decay profile quite satisfactorily. A comparative decay profile of transient absorption signals at 515 nm probe wavelength upon two different excitations with fluorescence decay profile at 670 nm is shown in Figure S18 &S19 for **Cor-AQ**

and **Cor–Fc** dyads, respectively. However, TA profile above 500 nm for both the dyads can nicely be fit with three components, of which first two components contributes 80- 90% of the decay and rest is contributed by third component whose lifetime (3.5 ns) is consistent with the S_1 decay of **TTC** and kept constant for the fitting (Figure 12). The fitting parameters are listed in Table 5 for both the excitations. The weighted average of first two decay times nicely corresponds to fluorescence decay of S1 state of dyads and it is ascribed to CS state.

The absorption spectrum of the radical anion of TPP/Zn-TPP, a typical tetrapyrrolic system, is composed of an intense Soret band red shifted by 10-20 nm than that of parent systems and a much weaker band just after Q band of the neutral parent system.[56] Similarly, the absorption spectrum of the radical cation of those systems do not differ much, with an intense band peaking after Soret band of neutral system and a weak and broad one after Q band of neutral system. TTC being a similar kinds of tetrapyrolic system, the characteristic absorption spectra of its radical anion or radical cation should contain an intense band in between 440-470 nm. As a consequence, in case of PET event in **Cor-Fc** or **Cor-AQ** dyads a clear absorption band was expected in TA absorption spectra in between 440-470 nm as signature of radical anion or radical cation formation respectively. However, TA spectra of neither **Cor-AQ** nor **Cor-Fc** show clear absorption for respective ions but change of peak position of transient absorption of singlet excited states as function of time and a sharp different time evolution of positive transient signals below 500 nm. This observation reveals that TA absorption in between 460 to 480 nm is the sum of absorption of radical ions and absorption of excited states and the decay of radical ions (charge recombination, CR) more or less follow the decay of transient absorption of singlet excited states. In view to estimate the CR time, we have analyzed the ground state bleaching signal at 435 nm for both the dyads upon S_2 and Q band excitations and shown in Figure 12. Like the decay of transient absorption of singlet excited states decay, ground state bleaching profiles are fit well by three components with short lifetime values and a long 3.5 ns component which was considered to be constraint of fitting. Resultant lifetime values of fitting analysis and corresponding amplitudes are placed in Table 5. Considering first two short components are due to charge recombination to the vibrationally hot ground state, the average time constant to CR is calculated to be 2-3 ps for **Cor-AQ** and 31-35 ps for **Cor-Fc**. Hence, respective CS and CR are found to be almost equal for both the dyads resulting non visibility of radical anion or cation spectra in TA spectra. In such circumstances, the observed CS population is levelled off due to CR as rise time of the CS band corresponds to the CR time constant and decay time of CS is CS time constant itself. Similar situation was encountered by Vauthey et al for porphyrin based system.[57] It is also important to mention that, CS and CR state are independent of excitation wavelength and this observation clearly reveals that electron transfer occurs in thermally equilibrium singlet state of corrole for both the dyads.

To enumerate the spectra and associated lifetimes of the states, we carried out global analysis [58] on the TA data of both dyads in ACN using the Glotaran software [59] applying a sequential model resulting in evolution associated difference spectra (EADS). Since, sequential model was used here to analyse TA data globally,

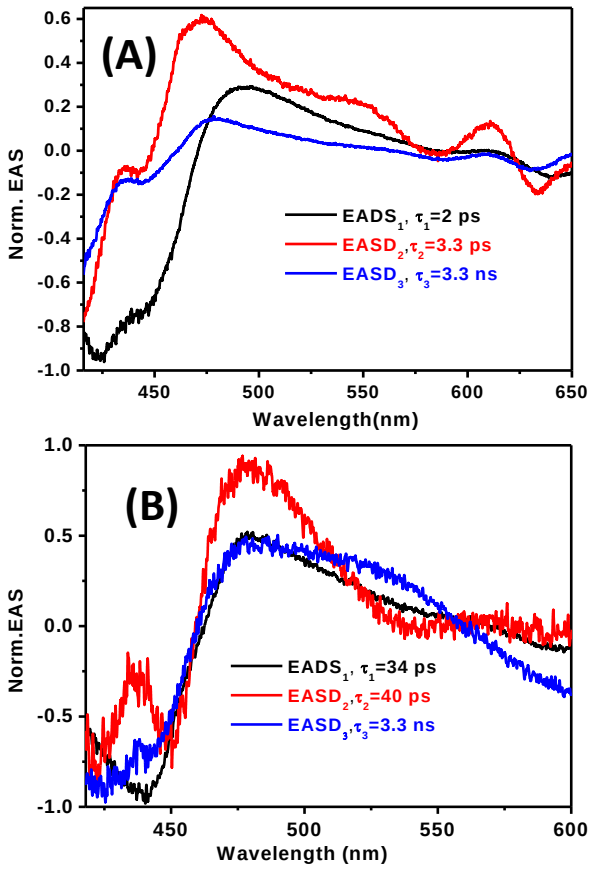

Fig. 13. Normalized Evolution-associated difference spectra (EADS) resulting from the global fitting applying a sequential model to the femtosecond transient absorption data of **Cor-AQ** (A) and **Cor-Fc** (B)

appeared EADS could represent a mixture of photophysical processes but one physical process to dominate a particular lifetime. Figure 13A &13B show the normalized EADS resulting from the global fit of the data for both the dyads (for absolute EADS see Figure S21). At least three exponential functions are necessary to fit globally for both the dyads and corresponding time constant nicely corroborate to the values obtained from the analysis of individual time profile of transient absorption of singlet excited states and ground state bleaching. The time constant of first component ($EADS_1$) coincides to the major component of fluorescence decay of the dyads as observed in FU study. Not only that, the spectral shape of the $EADS_1$ nicely corroborates to the TA spectra of simple TTC (Figure S22). Hence, $EADS_1$ can be assured to resemble to the excited state spectra and origin of the CS state. Since, a recombination channel of singlet states to the ground state occurring in parallel to charge separation, the time constant of $EADS_1$ obtained in this analysis presumably represents the lower limit of charge separation time and it is found to 2 ps for Cor-AQ and 34 ps for Cor-Fc respectively. The second component which has slightly higher time constant of 3.3 ps for Cor-AQ and 40 ps for Cor-Fc reflects the CS state and associated $EADS_2$ could predominantly correspond to the absorption spectra of respective radical ions of the dyads. As shown in Figure 13, the spectral shape of $EADS_2$ is clearly different than that of $EADS_1$. A new band in $EADS_2$ is

observed at around 464 nm for Cor-AQ and at 437 nm for Cor-Fc dyads. This new band in $EADS_2$ for respective dyads can be attributed to one of the peak of the absorption spectra of TTC radical cation and TTC radical anion spectra respectively. The third longest time constant is very similar for both the dyads and also very close to the S_1 fluorescence lifetime of TTC measured by TCSPC and corresponding $EADS_3$ indicates that the S_1 state population decays directly to the ground state or to the nearest triplet state (T_1). The shape of the $EADS_3$ for both the dyads closely resemblances to the shape of $EADS_1$ with little blue shift of excited state absorption peak and this can be ascribed due to some contribution of $T_n \leftarrow T_1$ transition to the $S_n \leftarrow S_1$ transition in this long time scale.

Overall, the aforesaid results unambiguously point to the following facts: (a) occurrence CS state for both the dyads, (b) CS state is faster in **Cor-AQ** than in **Cor-Fc** by more than one order, (c) CS and CR occur essentially with same time constants for the respective dyads. The free energy change for the CR calculated as $\Delta G_{CR} = E_{red}$ (Acceptor)- E_{ox}(Donor), found to be -1.17 and -1.30 eV for **Cor-AQ** and **Cor-Fc** dyads respectively. Hence, it could apparently be concluded that CR rate decreases on increasing free energy and CR occurs in Marcus Inverted region. However, the total reorganization energy (λ) of tetrapyrrolic systems was found to be of the order of 1-1.5 eV.[60] So, for both the dyads $-\Delta G_{CR}$ tends to be equal to λ, and CR occurs in Marcus optimal region, i.e. CR in both the dyads is essentially barrierless and rate of CR is thus ultrafast in nature. Since CR is barrier less process, its rate eventually is determined by CS rate. The CS and, therefore, CR in Cor-AQ occurs in 1-3 ps timescale which is very similar to the solvation in acetonitrile.[61] In such case, both CS and CR process are probably controlled the dielectric response of the solvents leading to the similar dynamic for CS and CR.[62]

Conclusions

We have designed and synthesized donor-acceptor systems based corrole-anthraquinone and corrole-ferrocene dyads using vinylic spacer. Both the dyads have been characterized by using various analytical tools. The ground state properties indicate modest interactions between corrole macrocycle and either anthraquinone or ferrocene moieties in both the dyads. Steady-state and fluorescence up-conversion studies revealed that **Cor-AQ** undergoes rapid electron transfer from singlet state of corrole to anthraquinone and from ground state of ferrocene to the first excited state of corrole in **Cor-Fc.** The electron transfer rates (or charge separation rates) for **Cor-Fc** and **Cor-AQ** were found to be 2.78×10^{10} and 3.33×10^{11} s^{-1}, respectively in acetonitrile solvent. Transient absorption studies indicate that respective charge separation and charge recombination occur in same timescale for both the dyads. Due to small energy gap between charge separated state and ground state, back electron transfer is barrier-less process and occurs too fast. These results also lead to established corrole as electron donor as well as electron acceptor depending upon the nature of attached other moiety.

Acknowledgements

We are grateful to Department of Science and Technology (DST, SB/S1/IC-14/2014) for financial support of this work. The author KS acknowledges University Grants Commission (UGC) for Senior Research Fellowship (SRF). PRB acknowledge P. Hemant Kumar for helping to collect fluorescence up-conversion as well as transient absorption data. We also thanks to Joris Snellenburg for seminal support in the usage of the Glotaran software.

Notes and references

1 A. C. Fahrenbach, C. J. Bruns, H. Li, A. Trabolsi, A. Coskun, A. F. Stoddart, *Acc. Chem. Res.* 2014, **47**, 482-493.
2 B. K. C. Chandra, G. N. Lim, V. N. Nesterov, P. A. Karr, F. D'Souza, *Chem. Eur. J.* 2014, **20**, 1-14.
3 L. Yuan, W. Lin, K. Zheng, S. Zhu, *Acc. Chem. Res*. 2013, **46**, 1462-1473.
4 J. H. Kim, M. Lee, J. S. Lee, Ch. B. Park, *Angew. Chem. Int. Ed.* 2012, **51**, 517-520.
5 D. Gust, T. A. Moore, A. L. Moore, *Acc. Chem. Res*. 2009, **42**, 1890-1898.
6 D. Gonzalez-Rodriguez, G. Bottari, *J. Porphyrins & Phthalocyanines* 2009, **13**, 624-636.
7 L. Flamigni, D. Gryko, *Chem. Soc. Rev*. 2009, **38**, 1635-1646.
8 F. D'Souza,; P. -M. Smith, M. E. Zandler, A. L. McCarty, M. Itou, Y. Araki, O. Ito, *J. Am. Chem. Soc*. 2004, **126**, 7898-7907.
9 L. Giribabu,; P. S. Reeta, R. K. Kanaparthi, M. Srikanth, Y. Soujanya, *J. Phys. Chem. A*. 2013, **117**, 2944-2951.
10 O. Ito, F. D'Souza, *Molecules* 2012, **17**, 5816-5835.
11 A. F. Mironov, Synthesis, Properties and Potential Applications of Porphyrins-Fullerenes. *Macroheterocycles* 2011, **4**, 186-208.
12 L. Giribabu, Ch. V. Kumar, P. Y. Reddy, *Chem. Asian J*. 2007, **2**, 1574-1580.
13 Smith, K. M.; Vicente, M. G. H. in Science of Synthesis, ed. Weinreb, S. M.; Georg Thieme Verlag, Stuttgart, New York, **2004**, 1081–1235.
14 Smith, K. M.; Vicente, M. G. H. in Science of Synthesis, ed. Weinreb, S. M.; Georg Thieme Verlag, Stuttgart, New York, **2004**, 1081–1235.
15 S.G. DiMagno, V. S. Y. Lin, M. J. Therien, *J. Org. Chem.* 1993, **58**, 5983.
16 J. Kandhadi, R. K. Kanaparthi, L. Giribabu, *J. Porphyrins & Phthalocyanines* 2012, **16**, 282-289.
17 A. de la Escosura, M. V. Martinez-Diaz, P. Thordarson, A. E. Rowan, R. J. M. Nolte, T. Torres, *J. Am. Chem. Soc*. 2003, **125**, 12300-12308.
18 A. Medina, C. G. Claessens, G. M. A. Rahman, A. M. Lamsabhi, O. Mó,; M. Yanez, D. M. Guldi, T. Torres, *Chem. Commun*. 2008, 1759-1761.
19 J. Ch. Lee, T.Y. Kim, S. H. Kang, Y. K. Shim, *Bull. Korean Chem. Soc.* 2001, **22**, 257.
20 H. Jia, B. Schmid, S. H. Liu, M. Jaggi, P. Monobaron, S. V. Bhosale, S. Rivadehi, S. J. Langford, L. Sanguinet, E. Levillain, M. E. El-Khouly, Y. Morita, S. Fukuzumi, S. Decurtins, *Chem.Phys.Chem*. 2012, **13**, 3370-3382.
21 S. Rai, M. Ravikanth, *Chem. Phys. Letts.* 2008, **453**, 250-255.
22 M. Stepien, B. Donnio, J. L. Sessler, *Angew. Chem. Int. Ed*. 2007, **119**, 1453-1457.
23 A. Osuka, E. Tsurumaki, T. Tanaka, *Bull. Chem. Soc. Jpn*. 2011, **84**, 679-697.
24 H. Maeda, H. A. Furuta, *Pure Appl. Chem*. 2006, **78**, 29-44.

25 B. C. Popere, A. M. D. Pelle, S. Thayumanavan, *Macromolecules* 2011, **44**, 4767-4776.
26 M. Tasior, D. T. Gryko, J. Shen, K. M. Kadish, T. Becherer, H. Langhals, B. Ventura, L. Flamigni, *J. Phys. Chem. C* 2008, **112**, 19699-19709.
27 C. M. Lemon, P. J. Brothers, *J. Porphyrins & Phthalocyanines* 2011, **15**, 809-834.
28 K. Sudhakar, V. Velkannan, L. Giribabu, *Tetrahedron Lett*. 2012, **53**, 991-993.
29 B. Ventura, A. DegliEsposti, B. Koszarna, D. T. Gryko, L. Flamigni, *New J. Chem*. 2005, **29**, 1559-1566.
30 J. Bendix, I. J. Dmochowski, H. B. Gray, A. Mahammed, L. Simkhovic, Z. Gross, *Angew. Chem., Int. Ed*. 2000, **39**, 4048-4051.
31 L. Giribabu, J. Kandhadi, R. K. Kanaparthi, *J. Fluorescence* 2014, **24**, 569-577.
32 L. Giribabu, J. Kandhadi, R. K. Kanaparthi, P. S. Reeta, *J. Luminescence* 2014, **145**, 357-363.
33 G. Rotas, G. Charalambidis, L. Galtzl, D. T. Gryko, A. Kahnt, A. G. Coutsolelos, N. Tagmatarchis, *Chem. Commun*., 2013, **49**, 9128-9130.
34 T. H. Ngo, F. Nastasi, F. Puntoriero, S. Campagna, W. Dehaen, W. Maes, *Euro. J. Org. Chem*. 2012, 5605-5617.
35 F. D'Souza, R. Chitta, K. Ohkubo, M. Tasior, N. K. Subbaiyan, M. E. Zandler, M. K. Rogacki, D. T. Gryko, S. Fukuzumi, *J. Am. Chem. Soc*. 2008, **130**, 14263-14272.
36 M. Tasior, D. T. Gryko, J. Shen, K. M. Kadish, T. Becherer, H. Langhals, B. Ventura, L. Flamigni, *J. Phys. Chem. C* 2008, **112**, 19699-19709.
37 M. Tasior, D. T. Gryko, M. Cembor, J. S. Jaworski, B. Venturac, L. Flamigni, *New. J. Chem.* 2007, **31**, 247-259.
38 L. Giribabu, K. Sudhakar, R. K. Kanaparthi, G. Sabapathi, *J. Photochem. Photobiol. A: Chem.* 2014, **284**, 18-26.
39 M. E. El-Khouly, S.Y. Shaban, O. Ito, N. Jux, *J. Porphyrins & Phthalocyanines* 2007, **11**, 719-728.
40 D. Curiel, K. Ohkubo, J. R. Reimers, S. Fukuzumi, M. J. Crossley, *Phys. Chem. Chem. Phys.* 2007, **9**, 5260-5266.
41 B. Koszarna, D. T. Gryko, *J. Org. Chem*. 2006, **71**, 3707-3717.
42 L. Zhang, S. Zeng, L. Yin, C. Ji, K. Li, Y. Li, *New J. Chem.* 2013, **37**, 632-639.
43 L. Giribabu, C. V. Kumar, V. G. Reddy, P. Y. Reddy, Ch. S. Rao, S. R. Jang, J. H. Yum, M. K. Nazeeruddin, M. Gratzel. *Sol. Energy Mater. Sol. Cells* 2007, **91** 1611-1617.
44 Gaussian 09 Revision A.01, M. J. Frisch, G. W. Trucks, H. B. Schlegel, G. E. Scuseria, M. A. Robb, J. R. Cheeseman, G. Scalmani, V. Barone, B. Mennucci, G. A. Petersson, *Gaussian, Inc., Wallingford CT*, 2009.
45 P. H. Kumar, Y. Venkatesh, D. Siva, B. Ramakrishna, P. R. Bangal, *J. Phys. Chem. A.* 2015, 119, 1267-1278.
46 W. W. Wadsworth, W. D. Emmons, *J. Am. Chem. Soc*., 1961, **83**, 1733-1738.
47 D. T. Gryko, J. Piechowska, J. S. Jaworski, M. Galezowski, M. Taisor, M. Cembor, H. Butenschon, *New. J. Chem.* 2007, **31**, 1613-1619.
48 J. Bendix, I. J. Domochowski, H. B. Gray, A. Mahammed, L. Simkhovich, Z. Gross, *Angew. Chem. Int. Ed.* 2000, **39**, 4048-4051.
49 M. Mastronian, W. Zhu, M. Stefenalli, S. Nardis, F. R. Fronczek, K. M. Smith, Z. Ou, K. M. Kadish, R. Paolesse, *Inorg. Chem.*, 2008, **47**, 11680-11687.
50 J. S. Baskin, H. Z. Yu, A. H. Zewail, *J. Phys. Chem. A.* 2002, **106**, 9837-9844.
51 H. Z. Yu, J. S. Baskin, A. H. Zewail, *J. Phys. Chem. A.* **2002**, *106*, 9845-9854.
52 R. A. Marcus, N. Sutin, Biochim. Biophys. Acta, 1985, **811**, 265-322.
53 N. Banerji, S. V. Bhosale, I. Petkova, S. J. Langford, E. Vauthey, *Phys. Chem. Chem. Phys*. 2011, **13**, 1019-1029 (and references therein).
54 P. T. Anusha, D. Swain, S. Hamad, L. Giribabu, T. S. Prashant, S. P. Tewari, S. V. Rao, *J. Phys. Chem. C* 2012, **116**, 17828-17837.
55 L. Zhang, Z. Y. Liu, X. Zhang, L. -L. Wang, H. Wang, H. -Y. Liu, Photochemical & Photobiol. Sci. **2015**, DOI: 10-1039/C5PP000060B.
56 S. K. Suguna, B. Robotham, R. P. Sloan, J. Szmytkowski, K. P. Ghiggino, M. F. Paige, R. P. Steer, *J. Phys. Chem. A* 2011, **115**, 12217-12227.
57 A. Morandeira, L. Engeli, E. Vauthey, *J. Phys. Chem. A* 2002, **106**, 4833-4837.
58 I. H. M. van Stokkum, D. S. Larsen, R. van Grondelle, *Biochimica Biophysica Acta* 2004, **1657**, 82-104.
59 J. J Snellenburg; S. P Laptenok; R. Seger; K. M. Mullen; I. H. M. van Stokkum, *J. Stat. Soft.* 2012, **49**, 1-22.
60 S. Prashanthi, P. H. Kumar, L. Wang, A. K. Perepogu, P. R. Bangal, *J Fluoresc* 2010, **20,** 571-580.
61 M. L. *Horng*, J. A. Gardecki, A. Papazyan, M. Maroncelli, *J. Phys. Chem*., 1995, **99**, 17311-17337.
62 I. Rips, J. Jortner, *J. Chem. Phys*., 1988, **88,** 818.